A numerical study of local traffic volume and air quality within urban street canyons

Huanhuan Wang [a], Peter Brimblecombe [b], Keith Ngan [a],*

[a] School of Energy and Environment, City University of Hong Kong, Kowloon, Hong Kong Special Administrative Region
[b] Department of Marine Environment and Engineering, National Sun Yat-Sen University, Kaohsiung, Taiwan

HIGHLIGHTS

- Local air quality is not determined solely by local traffic volume along a street.
- Simulated concentrations show good agreement with in situ roadside measurements.
- Emissions within the radius of homogenisation cannot be neglected.
- Pedestrianisation may not improve local air quality significantly.

GRAPHICAL ABSTRACT
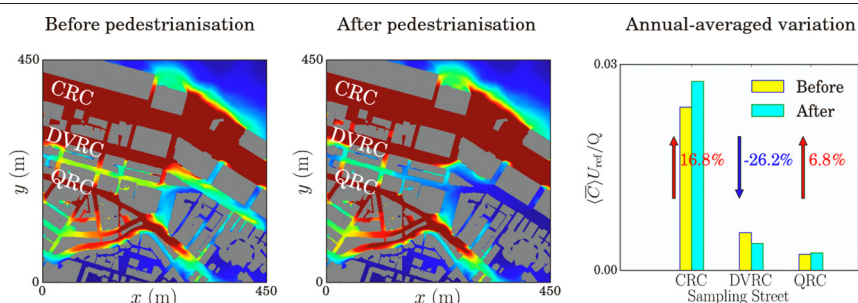
ARTICLE INFO

ABSTRACT

Although pollutant sources are often assumed to be spatially uniform, traffic in real cities may vary significantly in space. Consequently the local air quality within a street may not be determined solely by the traffic volume of the street. Using building-resolving large-eddy simulation, the relationship between traffic volume and air quality is investigated in the context of two idealised problems: (i) the influence of pollutants emitted from a main road on the surrounding side streets and (ii) the pedestrianisation of a central thoroughfare. It is shown that the spatial variation of traffic volume is of crucial importance within a near-field region defined by a radius of homogenisation (RAD). Furthermore, the actual impact depends strongly on the wind direction. Hence the benefits of pedestrianisation may be limited: for example, after removing 100% of the traffic along a street in a central business district, the annual-averaged local concentration decreases by ~30% when the urban background is neglected. The impact may be significantly lower when the background concentration is considered. This work is relevant to the formulation of effective traffic control policy and the improved understanding of spatially inhomogeneous pollutant sources.

© 2021 Elsevier B.V. All rights reserved.

1. Introduction

The importance of vehicular emissions for pedestrian-level air quality is well-established (Fenger, 1999; Colvile et al., 2001). It is often assumed that decreasing traffic volume will improve air quality within a local region of interest (e.g. a street or a neighbourhood; Zhang and Batterman (2013)). This expectation has helped spur the introduction of low (or zero) emission strategies (Geels, 2012; Emberger, 2017),

which have been implemented in many places, e.g., Singapore (Chin, 1996), California (Shaheen et al., 2002) and London (Beevers and Carslaw, 2005; Atkinson et al., 2009). It has also been cited as partial justification for the pedestrianisation of major thoroughfares (Pitsiava-Latinopoulou and Basbas, 2000; Hong Kong Institute of Planners, 2014).

In practice, however, the relationship between traffic volume and air quality is more complicated. While previous studies support the creation of car free cities (Nieuwenhuijsen and Khreis, 2016), there are mixed results for less ambitious strategies. Congestion charge schemes may not yield better air quality, though this was never their primary objective (Beevers and Carslaw, 2005; Atkinson et al., 2009). Analyses of

roadside pollutant concentrations before and after Hong Kong streets were blocked by protests indicate that statistically significant differences are difficult to discern (Brimblecombe and Ning, 2015; Brimblecombe, 2020).

Aside from regional influences (Brimblecombe and Ning, 2015), the effectiveness of a traffic-control strategy for improving air quality is constrained by two related issues. First, traffic control strategies may not eliminate traffic but instead divert it to neighbouring streets; thus their actual impact within the low-traffic region could be modest. Second, the influence of neighbouring streets may dominate over changes to the local traffic. These issues raise the question of the horizontal range over which a pollutant source exerts a significant influence. Field measurement results in the Whampoa neighbourhood of Hong Kong indicate that hourly-averaged $PM_{2.5}$ concentrations show a similar time evolution across several sites even though the local traffic volume decreases noticeably along the main road only (Wang et al., 2020). This suggests that the pollutant concentrations along quiet side streets may be determined largely by the main road; however, the precise reasons are unclear. There is limited understanding of how spatially varying traffic may affect pollutant dispersion within real cities, where the flow is strongly inhomogeneous. Most modelling studies of urban pollutant dispersion assume spatially uniform sources, though the influence of source location has been examined by a few authors (Kastner-Klein and Plate, 1999; Huang et al., 2015; Duan et al., 2019).

The relationship between local traffic volume and local air quality is investigated in this work using computational fluid dynamics (CFD), which is a valuable tool for studying the physical processes governing urban pollutant dispersion. After reviewing the methodology and describing detailed comparisons with roadside measurements (Sec. 2), the influence of local traffic volume is examined in two contexts: a busy road in the Whampoa neighbourhood (Sec. 3) and a proposed pedestrianisation scheme for Hong Kong's central business district (Sec. 4). The results are interpreted with respect to the radius of homogenisation, the lengthscale over which near-field effects are important (Kastner-Klein and Plate, 1999). The contribution of the urban background concentration is assessed in Sec. 5. The main findings are summarised in Sec. 6.

2. Methodology

2.1. Numerical model

Building-resolving simulations are performed using the parallelized large-eddy simulation (LES) model, PALM (Maronga et al., 2015), which has been applied to street canyons (Duan et al., 2019), building arrays (Lau and Ngan, 2018) and realistic urban areas (Park et al., 2015). The model is based on the non-hydrostatic, implicitly filtered, incompressible Navier-Stokes equations under the Boussinesq approximation. Defining the implicit filtering operation (denoted with the tilde) by

$$\tilde{\phi}(x_i, t) = \int_D F(x_i, x_i') \phi(x_i', t) dx_i', \tag{1}$$

where the filter function F represents the effect of the computational grid, ϕ is an arbitrary variable and D is the flow domain, the governing equations for the (resolved-scale) momentum, mass, and passive scalar take the form

$$\frac{\partial \widetilde{u_i}}{\partial t} + \frac{\partial \widetilde{u_i}\widetilde{u_j}}{\partial x_j} = -\frac{1}{\rho_0}\frac{\partial \widetilde{\pi}^*}{\partial x_i} - \frac{\partial}{\partial x_j}\left(\tau_{ij} - \frac{2}{3}e\delta_{ij}\right), \tag{2a}$$

$$\frac{\partial \widetilde{u_i}}{\partial x_i} = 0, \tag{2b}$$

$$\frac{\partial \tilde{c}}{\partial t} + \frac{\partial \widetilde{u_i}\tilde{c}}{\partial x_i} = \kappa \frac{\partial^2 \tilde{c}}{\partial x_i^2} - \frac{\partial \widetilde{u_i^* c^*}}{\partial x_i} + Q_0. \tag{2c}$$

Here $x_i = (x, y, z)$ are Cartesian directions and ρ_0 is the density of dry air. The asterisk denotes subgrid-scale (SGS) variables, i.e., $u_i^* = u_i - \tilde{u}_i$ is the SGS velocity and $\tau_{ij} = \widetilde{u_i u_j} - \widetilde{u}_i \widetilde{u}_j$ is the SGS stress tensor; the modified perturbation pressure $\widetilde{\pi}^* = \tilde{p}^* + \frac{2}{3}\rho_0 e$, with $\tilde{p}^*$ being the perturbation pressure and $e = \frac{1}{2}\widetilde{u_i^* u_i^*}$ being the subgrid-scale turbulent kinetic energy (TKE). c is the passive scalar (pollutant concentration), with turbulent diffusivity κ and volume source flux Q_0 (units: mass × volume^{-1} × time^{-1}); $\widetilde{u_i^* c^*}$ is the resolved-scale SGS scalar flux. Neutral flow and passive-scalar dynamics are assumed.

The advection terms are discretised using an upwind-biased 5th-order differencing scheme and the diffusion terms are discretised using 2nd order central difference, in combination with a 3rd-order Runge-Kutta time-stepping scheme (Williamson, 1980). The Deardorff (1980) scheme is used for subgrid-scale terms. The Poisson equation for pressure is solved with a fast Fourier transform.

2.2. Computational domain

The simulations are conducted for two Hong Kong neighbourhoods: Whampoa (Sec. 3) and Central (Sec. 4). The computational domain for the Whampoa neighbourhood is shown in Fig. 1a. This neighbourhood, which is composed largely of high-rise residential buildings, has an average aspect ratio, $AR \equiv H/W > 1$, where $H = 40$ m is the mean building height and W is the mean street width, and domain dimensions are 480 m × 480 m × 240 m in the x (streamwise), y (spanwise) and z (vertical) directions, respectively. The isotropic grid spacing is $\Delta = 1$ m. The external wind direction is northerly, which corresponds to the daily averaged background meteorological conditions on 27 September 2018.[1] The measurement sites are located on the sidewalks, immediately next to the streets.

A plan view of the Central domain is shown in Fig. 1b. Central, which is one of the busiest commercial areas in Hong Kong, features heavy traffic, high pedestrian volume, and tall high-rise buildings which conspire to create deep street canyons with average aspect ratio (building height to street width) greater than 1. The domain dimensions are 720 m × 720 m × 240 m in the x (streamwise), y (spanwise) and z (vertical) directions, respectively. The spatial resolution is isotropic, i.e. $\Delta = 1$ m.

2.3. Configuration

The flow is forced by a constant external pressure gradient, which is rotated to obtain a specific wind direction. In agreement with the annual-averaged mean wind speed at the Hong Kong Observatory's King's Park station, the mean wind speed at a height of ~40 m is 3.6 m s^{-1}. Periodic boundary conditions are applied in the horizontal to all variables; to avoid the accumulation of scalar within the computational domain, a sponge layer is introduced at the lateral edges (i.e. the concentration is manually reset to zero following each timestep). A free-slip boundary condition is imposed at the top of the computational domain. At solid surfaces, there is no slip for the velocity and Neumann for the scalar. A constant-flux layer with roughness length $z_0 = 0.1$ m is used for the wall function. Building data were obtained from the Hong Kong Lands Department.[2]

The passive scalar is released at ground level. The areal source flux, Q_i (units: mass × area^{-1} × time^{-1}) is constant within each street, i.e. $Q_i = Q_{0,i}\Delta z$ where Δz is the vertical grid spacing, $Q_{0,i}$ is the volume source flux and i labels the street. For simplicity, the source amplitudes are assumed to be directly proportional to the traffic volume, i.e. $Q_{0,i} = \varepsilon N_i$ where N_i is the number of vehicles passing along the street per unit time and ε is an emission factor (units: mass × volume^{-1} × vehicles^{-1}). Separate simulations are performed for each street or uniform area source: since the advection-diffusion equation (Eq. (2a)) is linear, this allows the scalar

---

[1] This wind direction is listed incorrectly in Table B-1 of Wang et al. (2020).
[2] https://www.landsd.gov.hk/mapping/en/digitalmap/3DBIT00.htm.
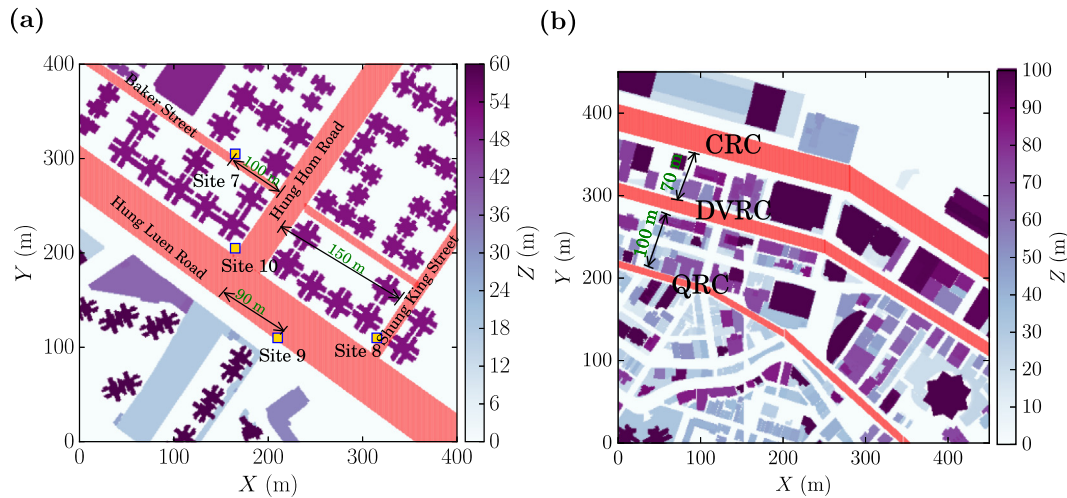
Fig. 1. Plan view of the computational domains. (a) Whampoa; (b) Central. A passive scalar is released from uniform area sources (indicated by the red areas). Measurement sites for the Whampoa domain are indicated with yellow squares. (For interpretation of the references to colour in this figure legend, the reader is referred to the web version of this article.)

field for a general source distribution to be reconstructed via superposition. In Secs. 3 and 4, ε is assumed without loss of generality to be an arbitrary constant. The average source flux over a neighbourhood is calculated by summing over the streets, e.g. $Q = \sum_i Q_i A_i / \sum_i A_i$ where A_i is the total area of a street.

The model was spun up for approximately 10,800 s, which is sufficient for the root-mean-square velocity and mean concentration to reach statistical stationarity in all cases. Afterwards data were collected for another 7200 s, which is long compared to the time required for a fluid parcel to be advected from one end of the computational domain to the other (~300 s). Only time-averaged data, indicated by the overbar, are considered. The vertical average over the mean depth of the canopy, i.e. $z/H \leq 1$ where H is the mean building height, is indicated by $\langle \cdot \rangle_H$. A volume average along a street for $10\,\text{m} < z < H$ is indicated by $\langle \cdot \rangle$.

2.4. Validation

PALM has been validated using wind-tunnel measurements of turbulence and scalar statistics, e.g. for flow over a street canyon (Lo and Ngan, 2015) and a regular building array (Lau and Ngan, 2018). In these calculations, a constant ground-level scalar source is applied and the statistically steady flow is forced by a constant pressure gradient. Validation using real urban measurements is less straightforward; nevertheless, Reynolds-Averaged Navier-Stokes (RANS) simulations have been successfully compared to air quality monitoring stations. For example, Santiago et al. (2017) obtained good agreement by allowing for variations in the inflow wind speed and calibrating against the time-mean pollutant concentrations. Scaling the simulated concentrations by a constant calibration coefficient partially compensates for discrepancies between the idealised numerical configuration and the real urban environment. Gallagher (2016) showed that NO_x concentrations measured by an elevated sensor (at a height of 8 m) can be estimated from LES after calibration for fleet composition and consistency with the measured concentration. Lauriks et al. (2021) compared predictions from an improved CFD model to pedestrian-level measurements of PM_{10} within a street canyon.

We now present a comparison of simulated and measured concentrations for the Whampoa and Central domains. In the former case, the measurements are taken from Wang et al. (2020), who measured the roadside $PM_{2.5}$ using portable pollution monitors. The numerical configuration is described in Sec. 3. In the latter case, the data are taken from Rakowska et al. (2014), who used a mobile monitor mounted to a bus at a height of approximately 2.5 m above ground level to record on-road $PM_{2.5}$ concentrations over several days. The

numerical configuration (Sec. 4.1) is modified to be consistent with the measurement conditions: the pollutant emissions are specified according to the traffic volumes (Supplementary Material, Table S.1) and the Euro 6 emission standard (Supplementary Material, Table S.2). The associated pedestrian-level winds are compared in Fig. S.1: the simulated and measured wind speeds show good agreement (with correlation coefficient $R \sim 0.78$).

As there are only three data points for the Central domain, statistical analysis is omitted; however, concentration time series for the three roads may be compared anyway (Supplementary Material, Fig. S.2). Relatively poor agreement is obtained using the results at the measurement height, $z = 2.5\,\text{m}$, presumably because the boundary conditions for the simulations and measurements differ: whereas simulated near-ground concentrations are strongly influenced by the wall function at the ground, near-ground pollutant measurements reflect the presence of vehicles, which deflect the flow and generate vehicle-produced turbulence (e.g. He and Dhaniyala, 2011). Substitution of a line source for an area source does not improve the agreement greatly (not shown). There is better agreement when the simulated data are averaged over $z < 10\,\text{m}$, $10\,\text{m} < z < H$ or $0 < z < H$; for example, the normalised mean-square error decreases from $NMSE \sim 9\%$ for $z = 2.5\,\text{m}$ to $NMSE \sim 3\text{–}4\%$ for $10\,\text{m} < z < H$ and $0 < z < H$, respectively.

Displacing the averaging region away from the ground may partially account for differences in the sources: whereas the simulated concentrations are generated by a uniform area source, the roadside measurements reflect emissions from discrete moving vehicles. From a calculation of the radius of homogenisation (see Sec. 3.2) in the vertical direction, the near-field region for the Central and Whampoa domains extends to $z = 10\,\text{m}$ (not shown). Averaging away from the ground necessitates calibration to compensate for the mismatch in height; for the Central domain, the DVRC concentrations are prescribed using the corresponding measurement. Hereafter the results for $10\,\text{m} < z < H$ are used to represent pedestrian-level concentrations. Since the results for $z \leq H$ are essentially unchanged compared to $10\,\text{m} < z < H$, the latter is used to represent the effects of pedestrianisation (Sec. 4).

Time-mean concentrations for the different Whampoa measurement sites are also compared (Supplementary Material, Fig. S.3). Following Santiago et al. (2017), the calibration coefficient is calculated by ensuring that the time-mean concentration measured along a single street or at a single measurement site is identical to the corresponding time-mean LES concentration.[3] Air quality performance metrics

---

[3] The dimensionless calibration coefficients are 0.65, 0.97 and 1.12 for $z = 2.5\,\text{m}$, $z < 10\,\text{m}$ and $10\,\text{m} < z < H$, respectively.

Table 1
Statistical performance measures for the Whampoa simulations (cf. Supplementary Material, Fig. S.3). The statistics are calculated for all measurement sites (Fig. 1a) and calibrated against the time-mean concentrations for the busy main road (Site 10). Each row corresponds to a different (vertical) averaging region. A perfect simulation would have $FB = NMSE = 0.0$ and $MG = VG = R = FAC = 1.0$.

	FB	MG	NMSE	VG	R	FAC2
Whampoa ($z = 2.5$ m)	0.08	1.03	0.12	1.11	0.54	1.0
Whampoa ($z < 10$ m)	−0.05	0.89	0.08	1.09	0.91	1.0
Whampoa (10 m $< z < H$)	−0.05	0.90	0.07	1.09	0.91	1.0
Whampoa (0 m $< z < H$)	−0.05	0.89	0.07	1.09	0.91	1.0

(see Appendix A for definitions) for the Whampoa simulations are summarised in Table 1; the general level of agreement is broadly consistent with Santiago et al. (2017), who obtained $R \in [0.79, 0.93]$ and $NMSE \in [0.17, 0.19]$ for an air quality monitoring station located within a garden close to the sidewalk.

The present calculations ignore the time-dependent meteorology and urban background concentrations (see Sec. 5). Furthermore, they do not capture fluctuations arising from passing vehicles or pedestrians. Nevertheless, it is evident that the model is capable of capturing the contribution of local emissions to PM$_{2.5}$.

3. A busy road surrounded by quiet streets

The effect of a busy road on neighbouring streets is now investigated for the Whampoa neighbourhood (cf. Fig. 1a). According to the traffic counts in Wang et al. (2020), traffic volume is much higher along the main road (Hung Hom Road) than along the side streets (Supplementary Material, Table S.3). Furthermore, traffic along the main road decreases from 9:00 to 12:00 while it fluctuates slightly along the other streets. To investigate the effects of spatially and temporally varying traffic, simulations with different emission patterns were performed. Each run or emission pattern corresponds to the mean traffic volume over an hour (Table S.3).

3.1. Impact of the busy road

The evolution of the concentration from 9:00 to 12:00 is now considered. Since the concentration values are arbitrary, they are normalised by U_{ref}, a reference velocity (at $z/H = 3.5$), and the mean source flux, Q. For each emission pattern, the temporally and spatially averaged fields have a very similar appearance, with large concentrations over much of the domain (Fig. 2). The temporal evolution is obscured by the normalisation with respect to the time-dependent source flux. The
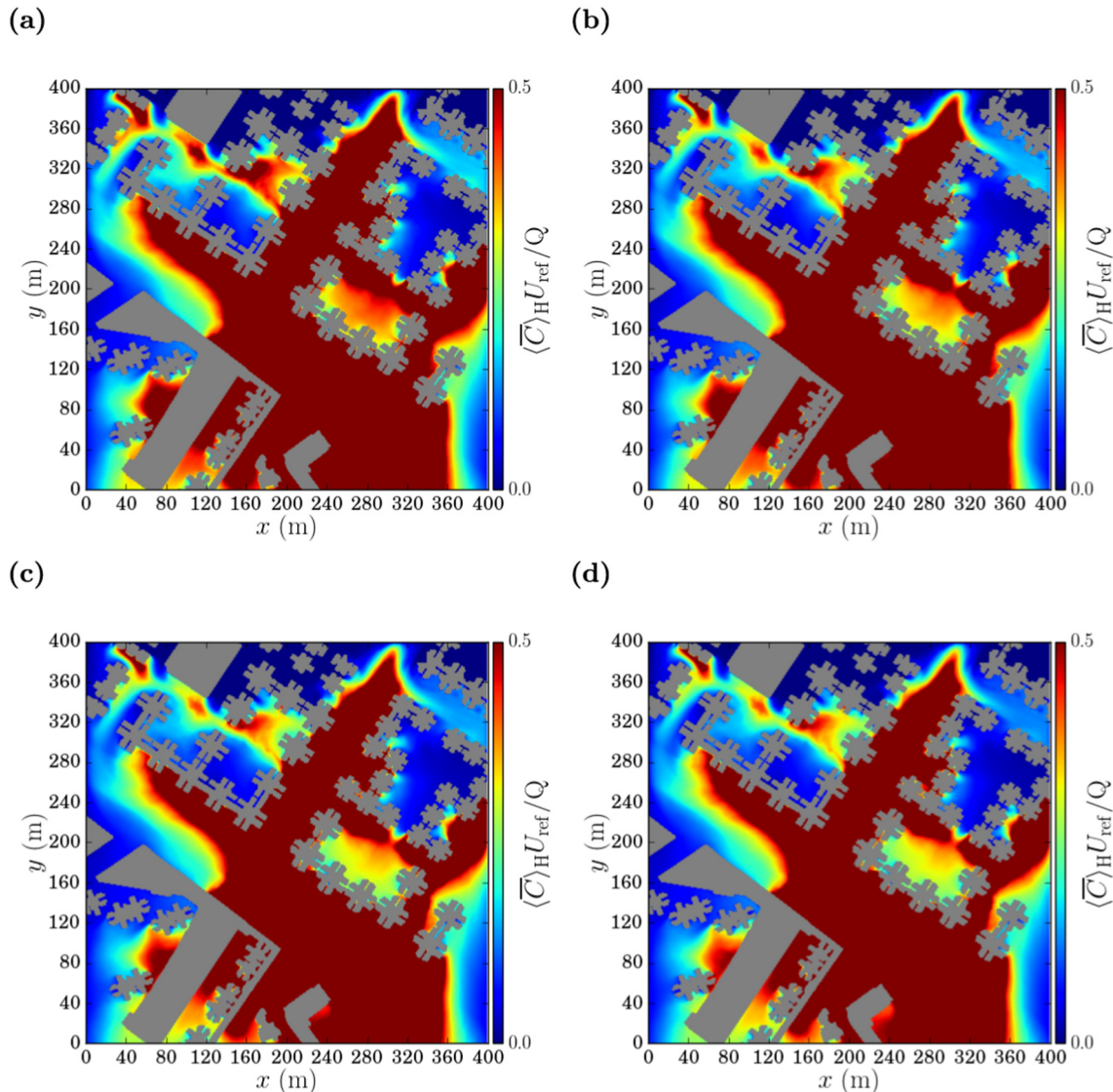
Fig. 2. Mean concentration fields for runs ending at (a) 9:00; (b) 10:00; (c) 11:00; (d) 12:00. Concentrations are averaged vertically over 10 m $< z < H$.

decrease in the concentrations is more easily seen in Fig. 3, which plots time series of the vertically-averaged concentrations for each emission pattern. The vertical average is required to avoid near-ground artifacts (see Sec. 2.4 for discussion). For each site, the simulated concentrations show reasonable agreement with the measured concentrations. The trends clearly reflect the influence of the decreasing traffic volume along the busy main road, but neither the measured nor simulated concentrations decrease at the same rate across the sites. The results show that the local air quality, e.g. an average along a street, may not be determined solely by local emissions. The implication is that the decreasing trend seen across all sites is related to spatial and temporal variations in traffic volume and pollutant emission.

3.2. Radius of homogenisation

Local traffic controls local air quality only in the absence of other factors, e.g., contributions from other streets. Clearly the contribution of a given pollutant source depends on the distance to the receptor. It will be negligible beyond a certain distance, but how is this crossover distance to be defined? In the pollutant dispersion literature, one sometimes distinguishes between a near-field region, in which pollutant concentrations depend sensitively on the details of the dispersion process and factors such as the building geometry, and a far-field region in which the sensitivity to these details is lost and a Gaussian-plume-like approximation may be applied (Plate and Baechlin, 1988). Alternatively the far field may be associated with the onset of central-limit-type behaviour (Belcher et al., 2015). Physically, a busy main road will influence neighbouring streets within the near field. Plate and Baechlin (1988) defined the near-field region, or equivalently a radius of homogenisation (RAD), by applying the Gaussian plume model (GPM; Stockie (2011)) to wind-tunnel data. The applicability of this approach to a real urban neighbourhood is not assured because the standard GPM assumes a flat surface (cf. Joseph et al., 2020). A universal definition of the RAD has yet to be proposed for urban flows.

We adopt a simple approach based on turbulence phenomenology (Lesieur, 2012). In homogeneous turbulence, the size of the large energetic eddies, the so-called integral scale, may be estimated from the spatial autocorrelation of the velocity. We define the RAD analogously. Denoting the spatial autocorrelation for the passive scalar concentration c as $\rho(r)$, the RAD is given by

$$RAD = \int_0^{R_{max}} \rho(r)dr, \tag{3}$$

where R_{max} is the largest horizontal scale. The spatial autocorrelation is obtained by integrating the two-point correlation over the domain (see Appendix B for details). Using LES data for flow over a cubic building array with external wind direction between 0° and 45°, Wang and Ngan (2021) observed that the mean concentration and spatial decay rate in the far field, $x > RAD$, show reduced sensitivity to the location of point sources within the repeating units of the array. In particular, the standard deviation of the spatial decay rates over an ensemble of point-source locations is approximately 10 times smaller in the far field. Furthermore, mean concentration differences for a spatially distributed source are approximately 4–8 times smaller in the far field. In the present context, Eq. (3) may be viewed as a reasonable definition of the scale over which concentrations are strongly correlated.

The RAD is calculated from a simulation in which emissions were limited to the main road. Volume-averaging over $z/H \leq 1$ yields RAD ~220 m. Since the distance between the main road and the side streets is around 100 m (cf. Fig. 1a), all measurement sites lie within the near-field region. Thus one may expect the concentration at each measurement site to be influenced by pollutant emissions along the main road. Given that the traffic volume along the main road is initially much greater, pollutant emissions from it strongly affect the concentrations at the measurement sites; the correlation is not perfect because the contribution from the side streets is not completely negligible (the ratio of the traffic volumes is ~3–5).

4. Pedestrianisation of a busy road

The impact of a pedestrianisation scheme on local air quality is examined in this section. It is not obvious a priori whether the impact is necessarily positive. From the results of Sec. 3, the impact could be modest if neighbouring streets lie in the near-field region. Following the analysis of Sec. 3, numerical simulations are analysed to address this issue.

Our study focuses on three busy roads (cf. Fig. 1b), Connaught Road Central, Des Voeux Road Central and Queen's Road Central. A brief description of their characteristics now follows:
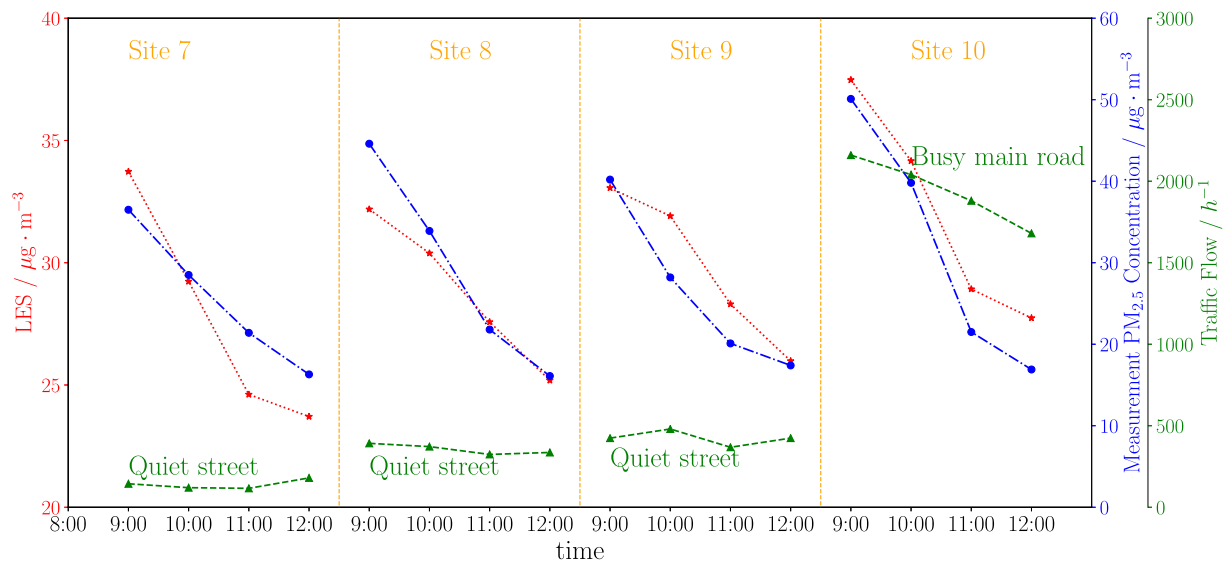
Fig. 3. Mean concentrations at the measurement sites of Fig. 1a on 27 September 2018. The LES data are averaged over 10 m < z < H. The LES results are shown in red and the field measurements (Wang et al., 2020) in blue. The traffic flow is presented in green. For the LES data, each point corresponds to a separate time-averaged run. (For interpretation of the references to colour in this figure legend, the reader is referred to the web version of this article.)

- *Connaught Road Central* (CRC). The studied section includes eight lanes, four in each direction. The north side is essentially open to Victoria Harbour; the south side is dominated by dense high-rise buildings. The average aspect ratio is ~ 2.
- *Des Voeux Road Central* (DVRC). DVRC runs parallel to CRC and is comprised of four traffic lanes, two in each direction, and two tram tracks. Both sides of the street are lined with dense high rise buildings. The average aspect ratio is ~ 5. The combination of narrow streets and tall buildings along both sides limit the dispersion of on-road emissions.
- *Queen's Road Central* (QRC). QRC has similar features to DVRC, but only two to three lanes in total. However, the building height is lower and the average aspect ratio is ~ 1.

4.1. Pedestrianisation scheme

The simulation procedure follows a pedestrianisation scheme proposed by Hong Kong Institute of Planners (Hong Kong Institute of Planners, 2014), which argues that pedestrianising DVRC would improve local air quality, among other benefits. There are two types of simulations:

1. *Before pedestrianisation*. Traffic volume for each of the three main roads is specified according to the Hong Kong Transport Department's estimate of daily traffic volume for 2018.[4]
2. *After pedestrianisation*. Traffic is eliminated completely from DVRC. For simplicity, it is assumed in the first instance that the DVRC traffic is diverted equally between CRC and QRC.

After pedestrianisation, the traffic volume of DVRC is reduced by 100%, while the traffic volume of CRC and QRC increases by 9% and 31% respectively. Traffic counts for the two (baseline) run types are summarised in Supplementary Material, Table S.4. For each run type, four different external wind directions are considered, i.e. westerly, northerly, easterly and southerly.

4.2. Impact of pedestrianisation

The qualitative influence of the pedestrianisation scheme may be easily grasped from the time-averaged pollutant fields (Fig. 4). Before pedestrianisation (top panels), high concentrations, shown in red, dominate. In the westerly and southerly cases, lower concentrations may be found in certain regions (as indicated by the regions in blue). For the easterly and northerly directions, however, the concentrations along the three streets show less spatial variability, notably along DVRC. The response is more complicated than the behaviour for idealised street-canyon flows, in which there is skimming flow and a coherent canyon circulation for a wind perpendicular to the canyon axis and channel flow for a wind parallel to the axis, because the street layout and building geometry are inhomogeneous. Whereas buildings are relatively tall towards the northeast corner (~ 80 m), they are shorter in the southwest (~ 50 m). The elucidation of the precise physical mechanisms is beyond the scope of this study, but it is evident that ventilation decreases under easterly and northerly winds.

After pedestrianisation (Fig. 4, bottom panels), lower concentrations may be seen. For the wind directions with better ventilation, i.e. the westerly and southerly cases, there is a dramatic decrease in concentrations along DVRC as the red areas are replaced with blue. For the wind directions with worse ventilation, i.e. the easterly and northerly cases, the impact is rather modest as high concentrations persist along DVRC even when emissions are restricted to CRC and QRC. These results imply that pedestrianisation does not necessarily have a significant effect.

The improvement may be quantified by comparing the mean concentrations along the streets (Fig. 5). In the absence of pollutant dispersion, there would be a 100% decrease along DVRC and 9% and 31% increases along CRC and QRC, respectively (cf. Table S.4). However, the mean concentrations along DVRC decrease by around 70% under winds favouring ventilation (westerly and southerly), but by only 20–30% for directions with poorer ventilation (easterly and northerly). The changes along CRC and QRC are not determined solely by the local emissions either. The concentration increase along CRC exceeds the increase in local emission for all wind directions, while the change along QRC is always smaller than the local increase in emissions.

The pedestrianisation impact over an entire year can be estimated from the wind rose, that is, from the probability of a specific wind direction. For simplicity, only the four cardinal wind directions are considered. (The contributions from other wind directions are reclassified via nearest-neighbour interpolation.) Letting $C^* \equiv \langle \overline{C} \rangle U_{\mathrm{ref}}/Q$ denote the normalised mean concentration, where U_{ref} is the constant reference speed at $z/H = 3.5H$, the annual average follows from

$$C_s^* = \sum_j p(\theta_j) C_s^*(\theta_j), \tag{4}$$

where s and j label the pedestrianisation scenario and wind direction, respectively. The wind rose for the Hong Kong Observatory's King's Park meteorological station[5] indicates that the most probable range of wind speeds is the same for the two most important cardinal wind directions (which occur over 80% of the time), thereby supporting the use of a constant inflow wind speed. Given this assumption, conclusions drawn from the annual average are unaffected by the normalisation; however, for the general situation in which the wind speed is not constant, this is no longer true.

The annual-averaged difference, $\Delta C^* = C_{\mathrm{after}}^* - C_{\mathrm{before}}^*$ and the normalised impact, $r_c = \Delta C^*/C_{\mathrm{before}}^*$, are now compared for the four wind directions. After pedestrianisation, the concentration decreases by an average of 26% along DVRC, but increases by 17% and 7% along CRC and QRC, respectively. See Supplementary Material, Table S.5 for a detailed comparison of the results for the different streets. The pedestrianisation impact averaged over the entire year is biased towards the low end of the responses depicted in Fig. 5 because easterly wind occurs nearly 70% of the time (Table S.5).

The mean local change in pollutant concentrations over an entire year is not well-predicted by the change in local emissions (Table S.4): air quality is worse than expected along DVRC and CRC, but better along QRC. Evidently pollutant dispersion from neighbouring streets plays an important role (cf. Fig. 4). The discrepancy between the local prediction and the mean local concentration may be related to pollutant trapping and the local building geometry. The mean aspect ratio is greatest for DVRC (~ 5) and lowest for QRC (~ 1). Thus one may expect pollutant trapping to be strongest (and ventilation weakest) for DVRC and the opposite for QRC; indeed DVRC concentrations always exceed QRC concentrations prior to pedestrianisation even though the traffic volume is lower along DVRC. This helps explain why air quality is worse than expected for DVRC but better for QRC. Since CRC features deep street canyons (i.e. mean aspect ratio ~ 2), it is also reasonable that air quality along CRC should be worse than expected from the local traffic volume.

In the foregoing, the external pressure gradient was chosen to yield a mean velocity scale that agrees with the annual average wind speed recorded by Hong Kong Observatory, $U_0 = 3.6$ m s^{-1} at $z = 40$ m. This wind speed lies near the lower end of the most probable range of wind speeds. We now consider the sensitivity to a wind speed at the top end of this range, i.e., $U_0 = 8.0$ m s^{-1} at $z = 40$ m. The normalised pedestrianisation impact, r_c, is approximately unchanged for CRC and

---

[4] https://www.td.gov.hk/filemanager/en/content4953/annual traffic census 202018.pdf.

[5] https://www.weather.gov.hk/en/cis/regionclimat/windrose.htm?&std=HKO.
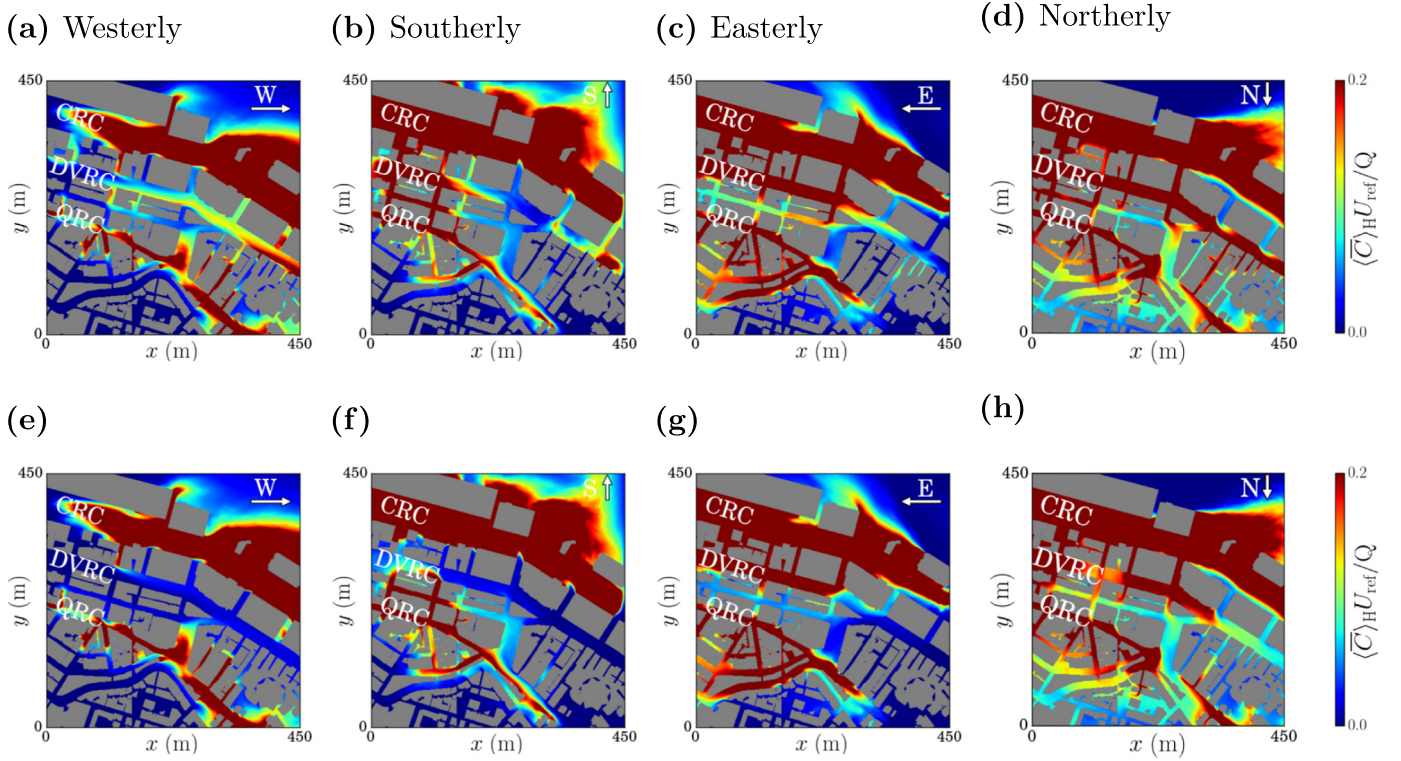
Fig. 4. Mean concentrations before (upper panels) and after (lower panels) pedestrianisation. The external wind direction is: (a,e) westerly; (b,f) southerly; (c,g) easterly; (d,h) northerly. As in Fig. 2, the time-averaged concentrations are averaged over 10 m ≤ z ≤ H, where H = 66 m is the mean building height. The mean source flux Q is a weighted average over the three streets.

QRC, the streets with a smaller AR (Supplementary Material, Table S.6); however, it doubles from 26% to 52% for DVRC. This response is not easily explained. While one may expect the increased wind speed to improve ventilation, thereby leading to a greater pedestrianisation impact, this is true only along DVRC under easterlies. Since the effect of the increased wind speed is maximised within a specific region (not shown), it is possible that the geometry and orientation of buildings play a role.

4.3. Influence of neighbouring streets

The behaviour described above is reminiscent of the Whampoa neighbourhood analysed in Sec. 3. To determine whether the potential impact of pedestrianisation is related to the proximity of the streets, the *RADs* are calculated. Since emissions from the streets are considered separately, this does not require additional simulations (see Sec. 2.3). The (volume-averaged) *RADs* for the three streets are around 200 m (see Supplementary Material, Table S.7). Since the distance between DVRC and its neighbours is around 100 m (Fig. 1b), this implies that DVRC is in the near-field region of the two side streets. This agrees with the finding that the impact of pedestrianisation is strongly affected by pollutant dispersion from neighbouring streets (Sec. 4.2).

The *RAD* characterises the range of scales over which neighbouring streets may exert an important influence, but does not quantify their contribution. Contributions to the local air quality within a given street may be determined from the simulations for each street or uniform area source. Fig. 6 compares contributions to the volume-averaged (10 m ≤ z ≤ H) DVRC concentration before pedestrianisation. For westerly and southerly winds, the local contribution dominates as ~75% of the air pollution in DVRC originates from DVRC. These are the directions for which ventilation is best and the local pedestrianisation impact greatest (Fig. 4). For easterly and northerly winds, the local contribution (~30–40%) is smaller than the one from CRC. These are the directions for which ventilation is worst and the local pedestrianisation impact attenuated.

4.4. Traffic optimisation

Fig. 6 confirms that the effects of pollutant emissions from the streets are not equal. This suggests that the traffic pattern may be optimised to minimise air pollution. In general,

$$\alpha_{CRC} + \alpha_{QRC} = 1, \tag{5}$$

where α_{CRC} and α_{QRC} denote the fraction of the DVRC traffic diverted into CRC and QRC. Since a passive scalar is linear in the source flux Eq. (2a), the contribution for arbitrary α_{CRC} or α_{QRC} may be obtained by scaling the results for a specified amplitude.

The mean concentrations vary linearly with α_{CRC} (Supplementary Material, Fig. S.4). For weak ventilation along DVRC (i.e. easterly and northerly winds), $\langle \bar{C} \rangle U_{ref}/Q$ increases with α_{CRC}: this suggests that pollutant dispersion from CRC to DVRC is favoured (cf. Fig. 6c and d). For strong ventilation along DVRC (i.e. southerly wind), the opposite situation occurs because there is enhanced dispersion from QRC to DVRC (cf. Fig. 6b). There is minimal sensitivity to the traffic allocation for westerly flow (cf. Fig. 6a) because the concentration is essentially insensitive to α_{CRC} when the external wind is nearly parallel to DVRC (cf. Fig. 4). Except for the southerly wind, C^* is minimised by setting $\alpha_{CRC} = 0$, i.e., diverting all of the traffic to QRC. The sensitivity to the source allocation is greatest for easterly and northerly winds and negligible for the westerly wind. The optimal source allocations are listed in Supplementary Material, Table S.8.

5. Effect of urban background concentrations

The calculations for the Whampoa (Sec. 3) and Central (Sec. 4) domains only consider local emissions. In reality, however, urban pollutant concentrations also depend on background values. If the background concentration, C_b, varies slowly in time, its influence on the time
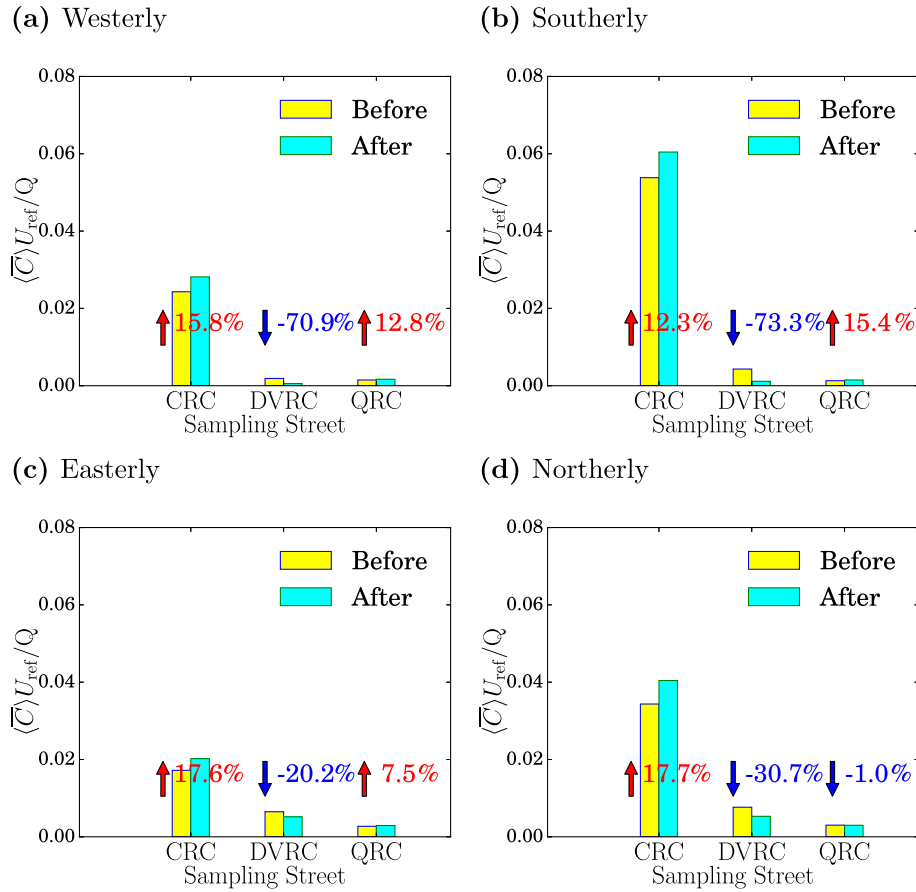
Fig. 5. Mean concentrations before and after pedestrianisation for the scalar fields of Fig. 4. The time-mean concentrations are averaged along the streets and 10 m ≤ z ≤ H. The response deviates significantly from the change in the local emissions (Table S.4).

evolution of the simulated concentrations can be neglected. The relatively good agreement, on timescales of 4 h or less, between the simulated and measured concentrations (Fig. 3) suggests that this assumption is satisfied for the Whampoa domain. On the other hand, background concentrations cannot be discounted in general. If C_b is sufficiently high, the actual effectiveness of a pedestrian scheme will be reduced. Thus the change in the mean concentrations calculated earlier (e.g. Fig. 5) represents an upper bound on the pedestrianisation impact.

The background concentration must be determined before the effect on pedestrianisation can be assessed. A simple solution is to choose sites that are in the far field of the emissions, but not so far from them as to be completely unrepresentative. This approach was employed by Brimblecombe and Ning (2015) and Brimblecombe (2020), who analysed the effect of road blockages by considering nearby urban sites. It is consistent with the notion that the urban background represents the pollutant distribution that would exist in the absence of local emissions.

Here we use measurements at the Environmental Protection Department's Central/Western and Central stations (Supplementary Material, Table S.9)[6] to estimate C_b for NO_2, NO_x, $PM_{2.5}$ and SO_2. Central/Western is representative of the far field and the urban background (cf. Table S.7): it is located approximately 900 m from QRC and 1100 m from DVRC. Central is representative of the near field: it is located on DVRC. Thus the contribution of local emissions from DVRC may be estimated by differencing the Central and Central/Western concentrations. For simplicity, the difference in measurement heights (16 m for Central/Western and 4.5 m for Central) is ignored. The ratio of the background

concentration to the total concentration along DVRC varies from a low of 30% for NO_x to a high of 98% for $PM_{2.5}$.

For non-zero background concentration, the estimate of the pedestrianisation impact is revised as follows. Given C_b and a contribution, C_l, arising from local emissions, the total concentration prior to pedestrianisation is

$$C_{before} = C_b + C_l. \tag{6}$$

After pedestrianisation, the total concentration, $C_{after} = C_{before} + \Delta C$, where ΔC represents the effect of eliminating local emissions. Hence the pedestrianisation impact

$$r = \frac{\Delta C}{C_{before}}. \tag{7}$$

In all cases, it is assumed that the pollutants are passive scalars, implying that local emissions of the different species have identical effects prior to scaling. A scaling factor, s, is determined by comparing the local concentration to the simulated volume-averaged concentration (10 m $< z < H$) within a street:

$$s = \frac{C_l}{\langle C \rangle}, \tag{8}$$

whence $\Delta C = s \langle \Delta C \rangle$.

Revised estimates of the pedestrianisation impact (cf. Fig. 6) are shown in Table 2. Given the assumption of passive scalar dynamics, differences in r arise solely from differences in C_b and C_l. Since the background contributions are very high for $PM_{2.5}$ and SO_2, pedestrianisation
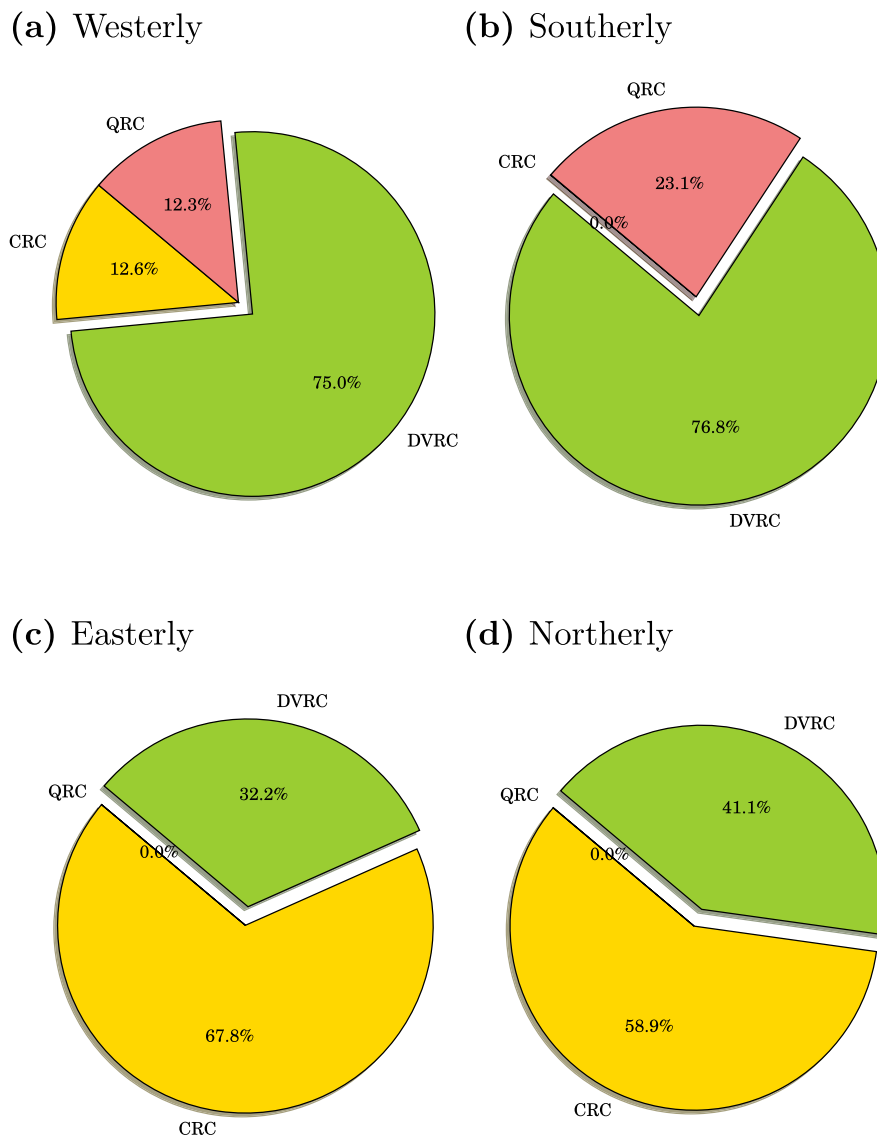

Fig. 6. Contribution of each street to DVRC air quality (i.e. time-mean concentrations averaged along the street and 10 m ≤ z ≤ H).

has little effect on them: the mean concentration along DVRC decreases by less than 1%. For NO_x and NO_2, the effect is larger, reaching 5% and 14%, respectively. Nonetheless the relative change in the total concentration is smaller than the upper bound of 26% that neglects the urban background (Table S.5). On the other hand, the increase in the concentrations along CRC and QRC is mitigated somewhat.

6. Conclusions

Local air quality along a street is not determined solely by the traffic volume of the street. Simulations for a busy road surrounded by quiet side streets show that local pollutant concentrations may be strongly influenced by emissions from neighbouring streets when they lie in the near field, i.e., within a radius of homogenisation estimated from spatial autocorrelations of the scalar concentrations. Predicted concentrations show relatively good agreement with in situ (approximately pedestrian level) roadside measurements when the spatial and temporal dependence of the emissions is taken into account. This suggests that the definition of local traffic volume should be expanded to include all sources within the near-field region. Simulations for a proposed pedestrianisation scheme indicate that the potential impact of eliminating local traffic may be limited. Since neighbouring streets may lie in the near field of the street to be pedestrianised, pollutant emission and dispersion from neighbouring streets may serve to lessen the potential impact from an elimination of local traffic. In practice, the actual impact depends on the wind direction and season as well as the traffic volume and pollutant. For Hong Kong's central business district, a reduction of ~20% in the annual-averaged NO_2 concentration and around 0.5% in $PM_{2.5}$ is obtained along the pedestrianised street when the annual-averaged wind speed is used. The theoretical maximum (for a passive scalar) is around 30% when the urban background is neglected.

These estimates have several limitations. First, it is assumed that the pollutants are passive scalars. Chemical reactions cannot be ignored for short-lived pollutants ([Harrison, 2018](#)), though the inclusion of

Table 2
Relative change, *r*, in the annual-averaged total concentration after pedestrianisation when the urban background is taken into account. For each of the species, Δ*C*, the volume average along the streets of the local concentration difference due to pedestrianisation (Supplementary Material, Table S.5), is scaled appropriately.

	NO_2	NO_x	$PM_{2.5}$	SO_2
CRC	8.6%	11.8%	0.3%	0.5%
DVRC	−13.3%	−18.3%	−0.5%	−0.8%
QRC	13.9%	4.8%	0.1%	0.2%

chemical reactions (e.g. Zhong et al., 2016) is computationally expensive. Given that numerical simulations of passive scalars are still widely used in the pollutant dispersion literature, the present results should serve as a useful bechmark for future studies of reactive pollutants. Second, processes such as wall heating (Cai, 2012), traffic-produced turbulence (He and Dhaniyala, 2011) or time-varying inflow boundary conditions (Duan and Ngan, 2018) are neglected. Since these processes enhance dispersion and mixing inside the urban canopy, one may expect the potential impact of pedestrianisation to be reduced. Third, a constant inflow wind speed is assumed. Although this is a reasonable first assumption for Hong Kong, in general one must contend with variations in the wind speed. This is important for averages over long and short timescales. In the latter case, fluctuations could serve to increase the instantaneous effect of pedestrianisation. Calculations with a characteristic inflow speed of $U_0 = 8 \text{ m s}^{-1}$ rather than 3.6 m s^{-1} indicate that the pedestrianisation impact increases by a factor of 2.5 for easterlies and 2 for the annual average.

The main finding of this work is that the effects of pedestrianisation (or more generally, near-field sources) are site specific or problem dependent. For example, the effect of decreasing local emissions or pedestrianisation would increase when there is good ventilation or winds that are roughly parallel to the street axis. Thus differences from an annual or seasonal average may be seen on shorter timescales.[7] Nevertheless, one may generally expect that changes in local air quality will not be directly proportional to changes in local traffic volume because pollutant dispersion cannot be ignored except in special cases. When ventilation is sub-optimal (on account, e.g., of the building geometry), pedestrianisation may not provide substantial environmental benefits; indeed it may have unintended side effects such as an increase in pollution along side streets caused by the diversion of traffic. The benefits of a pedestrianisation scheme for local air quality should be carefully assessed prior to implementation, perhaps with numerical simulations analogous to the ones described here.

CRediT authorship contribution statement

Huanhuan Wang: Writing – original draft, Software, Investigation, Validation, Visualization. **Peter Brimblecombe:** Conceptualization, Writing – review & editing. **Keith Ngan:** Supervision, Methodology, Formal analysis, Writing – review & editing, Project administration, Funding acquisition.

Declaration of competing interest

The authors declare that they have no known competing financial interests or personal relationships that could have appeared to influence the work reported in this paper.

Acknowledgements

Appendix A. Statistical metrics for validation

In order to validate the simulation data (D_s) against measurements (D_e), we calculate the following statistical performance measures (Chang and Hanna, 2004), which include the fractional bias (FB),

[7] http://www.hongkongcan.org/hk/article/14400-citizens-enjoyed-pedestrianised-dvrc-with-cleaner-air/.

$$FB = \frac{(\overline{D_e} - \overline{D_s})}{0.5(\overline{D_e} + \overline{D_s})}, \tag{A.1}$$

the geometric mean bias (MG),

$$MG = \exp\left(\overline{\ln D_e} - \left(\overline{\ln D_{se}}\right)\right), \tag{A.2}$$

the normalised mean square error ($NMSE$),

$$NMSE = \frac{\overline{(D_e - D_s)^2}}{\overline{D_e}\,\overline{D_s}}, \tag{A.3}$$

the geometric variance (VG),

$$VG = \exp\left[\overline{\left(\ln D_e - \ln D_s\right)^2}\right], \tag{A.4}$$

the correlation coefficient (R),

$$R = \frac{\overline{(D_e - \overline{D_c})(D_s - \overline{D_s})}}{\sigma_{D_e}\,\sigma_{D_s}}, \tag{A.5}$$

fraction of data ($FAC2$),

$$FAC2 = \frac{1}{N}\sum_{I=0}^{N-1}\chi_i, \text{ where } \chi_i = \begin{cases} 1, & \text{for } 0.5 \leq \frac{D_e}{D_s} \leq 2.0, \\ 0, & \text{otherwise,} \end{cases} \tag{A.6}$$

where the overbar represents average over the dataset and σ_{De}, σ_{Ds} are the standard deviations.

Appendix B. Calculation of the RAD

Let $c(R,\theta)$ denote the concentration at radial distance R and angle θ from an arbitrary origin. The 1-D radial autocorrelation is then given by

$$\rho(r;\theta,t) = \frac{\langle c(R)c(r+R)\rangle_R}{\sigma^2} \tag{B.1}$$

where $\langle\cdot\rangle_R$ is the average over R and σ is the standard deviation of c. For simplicity, homogeneity is assumed. To calculate the 2-D spatial autocorrelation, we average c over all directions and time to obtain $\langle c(R)\rangle_{\theta,\,t}$; points lying within buildings or outside the domain are excluded from the average. Hence

$$\rho(r) = \frac{\left\langle\langle c(R)\rangle_{\psi,t}\,\langle c(R+r)\rangle_{\psi,t}\right\rangle_R}{\hat{\sigma}^2}, \tag{B.2}$$

where the standard deviation is now given by

$$\hat{\sigma}(R) = \left\langle\left(\langle c\rangle_{\psi,t} - \widehat{\langle c\rangle}_{\theta,t}\right)^2\right\rangle_R, \tag{B.3}$$

with $\widehat{\langle c\rangle}_{\theta,t} \equiv \langle\langle c\rangle_{\theta,t}\rangle_R$. Similar results are obtained when c is averaged over θ only (not shown).

The RADs for the Central domain are listed in Table S.7.

Appendix C. Supplementary data

Supplementary data to this article can be found online at https://doi.org/10.1016/j.scitotenv.2021.148138.

References

Atkinson, R.W., Barratt, B., Armstrong, B., Anderson, H.R., Beevers, S.D., Mudway, I.S., Green, D., Derwent, R.G., Wilkinson, P., Tonne, C., et al., 2009. The impact of the congestion charging scheme on ambient air pollution concentrations in London. Atmos. Environ. 43 (34), 5493–5500.

Beevers, S.D., Carslaw, D.C., 2005. The impact of congestion charging on vehicle emissions in London. Atmos. Environ. 39 (1), 1–5.

Belcher, S.E., Coceal, O., Goulart, E.V., Rudd, A.C., Robins, A.G., 2015. Processes controlling atmospheric dispersion through city centres. J. Fluid Mech. 763, 51–81.

Brimblecombe, P., 2020. Street protests and air pollution in Hong Kong. Environ. Monit. Assess. 192 (5), 1–9.

Brimblecombe, P., Ning, Z., 2015. Effect of road blockages on local air pollution during the Hong Kong protests and its implications for air quality management. Sci. Total Environ. 536, 443–448.

Cai, X., 2012. Effects of differential wall heating in street canyons on dispersion and ventilation characteristics of a passive scalar. Atmos. Environ. 51, 268–277.

Chang, J.C., Hanna, S.R., 2004. Air quality model performance evaluation. Meteorog. Atmos. Phys. 87, 167–196.

Chin, A.T., 1996. Containing air pollution and traffic congestion: transport policy and the environment in Singapore. Atmos. Environ. 30 (5), 787–801.

Colvile, R., Hutchinson, E.J., Mindell, J., Warren, R., 2001. The transport sector as a source of air pollution. Atmos. Environ. 35 (9), 1537–1565.

Deardorff, J.W., 1980. Stratocumulus-capped mixed layers derived from a three-dimensional model. Bound.-Layer Meteorol. 18 (4), 495–527.

Duan, G., Ngan, K., 2018. Effects of time-dependent inflow perturbations on turbulent flow in a street canyon. Bound.-Layer Meteorol. 167 (2), 257–284.

Duan, G., Jackson, J.G., Ngan, K., 2019. Scalar mixing in an urban canyon. Environ. Fluid Mech. 19 (4), 911–939.

Emberger, G., 2017. Low carbon transport strategy in Europe: a critical review. Int. J. Sustain. Transp. 11 (1), 31–35.

Fenger, J., 1999. Urban air quality. Atmos. Environ. 33 (29), 4877–4900.

Gallagher, J., 2016. A modelling exercise to examine variations of NOx concentrations on adjacent footpaths in a street canyon: the importance of accounting for wind conditions and fleet composition. Sci. Total Environ. 550, 1065–1074.

Geels, F.W., 2012. A socio-technical analysis of low-carbon transitions: introducing the multi-level perspective into transport studies. J. Transp. Geogr. 24, 471–482.

Harrison, R.M., 2018. Urban atmospheric chemistry: a very special case for study. npj Clim. Atmos. Sci. 1 (1), 1–5.

He, M., Dhaniyala, S., 2011. A dispersion model for traffic produced turbulence in a two-way traffic scenario. Environ. Fluid Mech. 11 (6), 627–640.

Hong Kong Institute of Planners, 2014. Proposed Tram & Pedestrian Precinct in Des Voeux Road Central.

Huang, Y.D., Xu, X., Liu, Z.Y., Kim, C.N., 2015. Effects of strength and position of pollutant source on pollutant dispersion within an urban street canyon. Environ. Forensic 16 (2), 163–172.

Joseph, G., Hargreaves, D., Lowndes, I., 2020. Reconciling Gaussian plume and computational fluid dynamics models of particulate dispersion. Atmos. Environ. X 5, 100,064.

Kastner-Klein, P., Plate, E., 1999. Wind-tunnel study of concentration fields in street canyons. Atmos. Environ. 33 (24–25), 3973–3979.

Lau, G.E., Ngan, K., 2018. Analysing urban ventilation in building arrays with the age spectrum and mean age of pollutants. Build. Environ. 131, 288–305.

Lauriks, T., Longo, R., Baetens, D., Derudi, M., Parente, A., Bellemans, A., van Beeck, J., Denys, S., 2021. Application of improved CFD modeling for prediction and mitigation of traffic-related air pollution hotspots in a realistic urban street. Atmos. Environ. 246, 118,127.

Lesieur, M., 2012. Turbulence in fluids. 3rd edn. Springer.

Lo, K., Ngan, K., 2015. Characterising the pollutant ventilation characteristics of street canyons using the tracer age and age spectrum. Atmos. Environ. 122, 611–621.

Maronga, B., Gryschka, M., Heinze, R., Hoffmann, F., Kanani-Sühring, F., Keck, M., Ketelsen, K., Letzel, M.O., Sühring, M., Raasch, S., 2015. The parallelized large-Eddy simulation model (PALM) version 4.0 for atmospheric and oceanic flows: model formulation, recent developments, and future perspectives. Geosci. Model Dev. 8 (8), 2515–2551.

Nieuwenhuijsen, M.J., Khreis, H., 2016. Car free cities: pathway to healthy urban living. Environ. Int. 94, 251–262.

Park, S.B., Baik, J.J., Han, B.S., 2015. Large-eddy simulation of turbulent flow in a densely built-up urban area. Environ. Fluid Mech. 15 (2), 235–250.

Pitsiava-Latinopoulou, M., Basbas, S., 2000. The impact of pedestrianization schemes on the environmental quality at central areas. WIT Trans. Built. Environ. 49.

Plate, E., Baechlin, W., 1988. Wind tunnel tests as part of a warning system for accidental gaseous spills. J. Wind Eng. Ind. Aerodyn. 29 (1–3), 165–174.

Rakowska, A., Wong, K.C., Townsend, T., Chan, K.L., Westerdahl, D., Ng, S., Močnik, G., Drinovec, L., Ning, Z., 2014. Impact of traffic volume and composition on the air quality and pedestrian exposure in urban street canyon. Atmos. Environ. 98, 260–270.

Santiago, J., Borge, R., Martin, F., de la Paz, D., Martilli, A., Lumbreras, J., Sanchez, B., 2017. Evaluation of a CFD-based approach to estimate pollutant distribution within a real urban canopy by means of passive samplers. Sci. Total Environ. 576, 46–58.

Shaheen, S.A., Wright, J., Sperling, D., 2002. California's zero-emission vehicle mandate: linking clean-fuel cars, carsharing, and station car strategies. Transp. Res. Rec. 1791 (1), 113–120.

Stockie, J.M., 2011. The mathematics of atmospheric dispersion modeling. SIAM Rev. 53 (2), 349–372.

Wang, H., Ngan, K., 2021. Effects of Inhomogeneous Ground-level Pollutant Sources Under Dfferent Wind Directions. Preprint.

Wang, H., Brimblecombe, P., Ngan, K., 2020. Particulate matter inside and around elevated walkways. Sci. Total Environ. 699 (134), 256.

Williamson, J., 1980. Low-storage Runge-Kutta schemes. J. Comput. Phys. 35 (1), 48–56.

Zhang, K., Batterman, S., 2013. Air pollution and health risks due to vehicle traffic. Sci. Total Environ. 450, 307–316.

Zhong, J., Cai, X.M., Bloss, W.J., 2016. Coupling dynamics and chemistry in the air pollution modelling of street canyons: a review. Environ. Pollut. 214, 690–704.